

1 **Title: Stretchable pumps for soft machines**

2

3 Author's Accepted Manuscript version of

4 Cacucciolo V, Shintake J, Kuwajima Y, Maeda S, Floreano D, Shea H. Stretchable pumps for soft
5 machines. Nature. 2019 Aug; 572(7770):516–9.

6 DOI: 10.1038/s41586-019-1479-6

7 URL : <https://www.nature.com/articles/s41586-019-1479-6>

8

9 **Authors:** Vito Cacucciolo^{1*}, Jun Shintake^{2,3}, Yu Kuwajima⁴, Shingo Maeda⁴, Dario Floreano²,
10 Herbert Shea^{1*}

11 **Affiliations:**

12 ¹Soft Transducers Laboratory (LMTS), Institute of Microengineering, School of Engineering,
13 École Polytechnique Fédérale de Lausanne (EPFL), Rue de la Maladière 71b, 2000 Neuchâtel,
14 Switzerland.

15 ²Laboratory of Intelligent Systems (LIS), Institute of Microengineering, School of Engineering,
16 École Polytechnique Fédérale de Lausanne (EPFL), Route Cantonale, 1015 Lausanne, Switzerland.

17 ³Department of Mechanical and Intelligent Systems Engineering, School of Informatics and
18 Engineering, The University of Electro-Communications, 1-5-1 Chofugaoka, Chofu, 182-8585
19 Tokyo, Japan.

20 ⁴Smart Materials Laboratory, Department of Engineering Science and Mechanics, Shibaura
21 Institute of Technology, 3-7-5 Toyosu, Koto, 135-8548 Tokyo, Japan.

22 *Correspondence to: vito.cacucciolo@epfl.ch, herbert.shea@epfl.ch

23

24 **Text:**

25

26 **Machines made of soft materials bridge life sciences and engineering¹. Advances in soft**
27 **materials have enabled skin-like sensors and muscle-like actuators for soft robots and**
28 **wearables^{1–3}. Flexible or stretchable counterparts of most key mechatronic components have**
29 **been developed⁴, principally using fluidically-driven systems^{5–7}, though other mechanisms**
30 **have been reported⁸, including electrostatic^{9–12}, stimuli responsive gels^{13,14}, and thermally**
31 **responsive materials such as liquid metals^{15–17} and shape memory polymers¹⁸. Yet, there exist**
32 **to date very few soft counterparts of pumps or compressors, greatly limiting the portability**
33 **and autonomy of soft machines^{4,7}. We describe here a class of soft-matter bidirectional pumps**
34 **based on charge-injection ElectroHydroDynamics (EHD)¹⁹. These solid-state pumps are**
35 **flexible, stretchable, modular, scalable, noiseless, and fast. By integrating the pump in a**
36 **glove, we demonstrate wearable active thermal management. By embedding the pump in an**
37 **inflatable structure, we report a self-contained fluidic muscle. The stretchable pumps enable**
38 **the integration of fluidic circuits in any object, paving the way to wearable lab-on-a-chip and**
39 **microfluidic sensors, thermally active clothing, and autonomous soft robots.**

40
41 Despite the widespread use of fluidic actuation, there are very few soft counterparts of pumps or
42 compressors. Conventional pumps and compressors are bulky and rigid systems including
43 impellers, bearings, and electrical motors. They often require lubrication and produce noise. Even
44 miniaturized pumps (e.g., based on piezo-actuators or electrophoresis²⁰) are rigid and have moving
45 parts with very few exceptions (see Extended Data Table 1). The lack of electrically-powered
46 flexible or stretchable pumps greatly hinders many applications of fluid-driven soft-systems,
47 ranging from robotics and mechatronics (actuators and sensors) to biology (e.g., microfluidics for
48 cell cultures) to wearable devices (heat distribution).

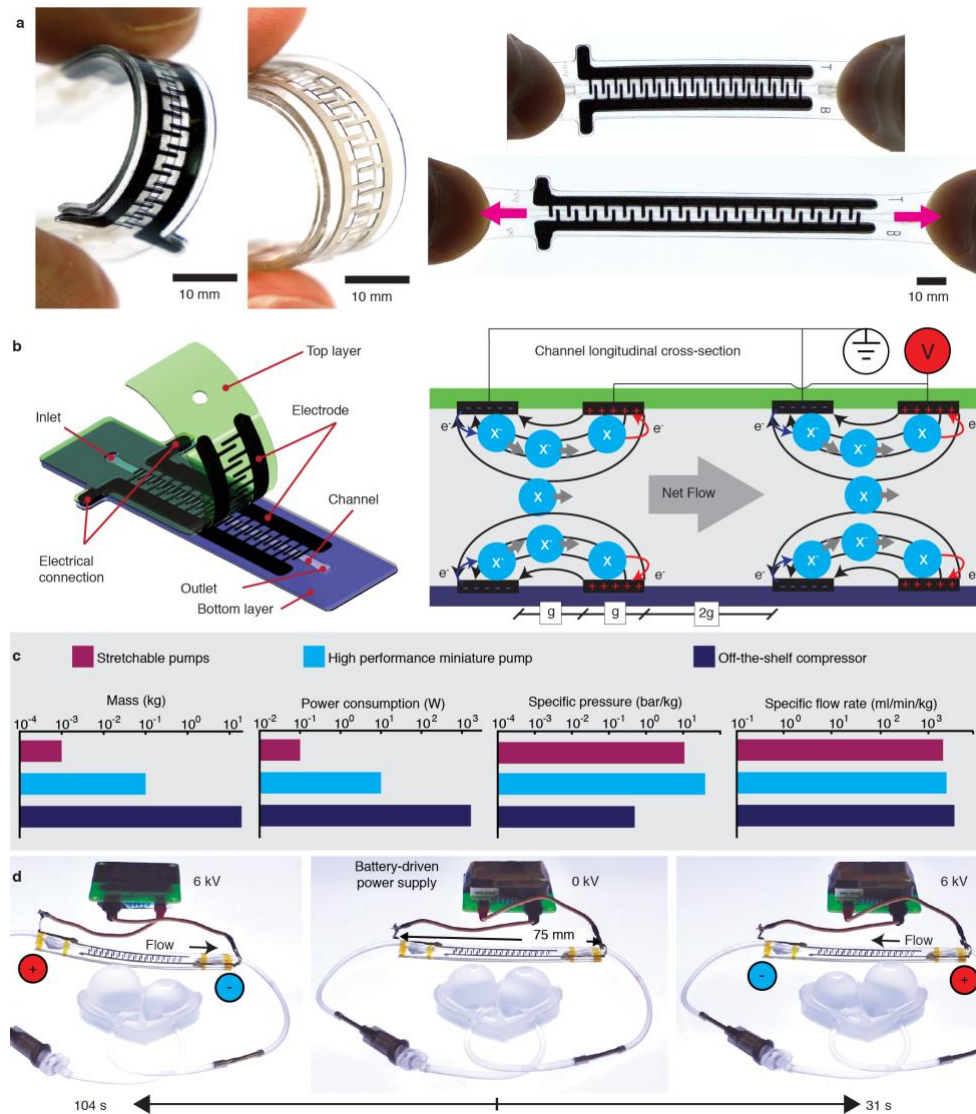


Fig. 1: Stretchable pumps based on charge-injection ElectroHydroDynamics (EHD). **a**, Pumps made with carbon (left) and silver electrodes (center) bent to a small radius of curvature and stretched to 50% (right). **b left**, Schematic diagram of the stretchable pump. The top and bottom layers are PDMS (Polydimethylsiloxane) membranes of thickness 0.4 mm, on which 30 μm thick compliant electrodes are patterned. The channel is a laser cut 0.5 mm thick PDMS layer. **b right**, Operating principle of the pump. Both top and bottom electrodes are interdigitated. The gap g between fingers of opposite polarity is 0.5 mm, and the spacing between finger pairs is 1 mm. The channel is filled with dielectric liquid. When the applied electric field exceeds a threshold of 5 to 8 $\text{V}/\mu\text{m}$, electrons tunnel from the cathode into the liquid. The resulting ions are accelerated by the electric field until they discharge at the anode, dragging neutral liquid along their path, leading to fluid flow. **c**, Performance comparison between the stretchable pumps, a miniature pump (TCS Micropumps, MGD 1000S) and an off-the-shelf compressor (McMaster, single tank portable air compressor) **d**, A demonstration of a stretchable pump moving liquid between two ventricles of a heart-shaped balloon. By changing the polarity of the applied voltage, the flow direction is reversed. The pump is driven by a 20 g battery-operated 6 kV power supply (see Supplementary Video 2).

50 In this work, we present a class of soft-matter pumps, consisting of a monolithic elastomer tube
51 with embedded compliant electrodes (Fig. 1a, Supplementary Video 1). The pumping mechanism
52 is charge-injection ElectroHydroDynamics (EHD): a dielectric fluid in the channel is accelerated
53 by means of a high DC electric field (6-12 V/ μm) (Fig. 1b), allowing pumping in both
54 directions^{19,21–25}. See Methods and Extended Data Fig. 1 for a description of the EHD mechanism
55 used in this work. Figure 1c shows a comparison between the stretchable pumps, a high-
56 performance miniature pump (TCS Micropumps, MGD 1000S), and a large off-the-shelf
57 compressor (McMaster, single tank portable air compressor), both commonly used to power soft
58 fluidic actuators²⁶. Figure 1d and Supplementary Video 2 show the stretchable pump moving liquid
59 between two ventricles of a heart-shaped balloon, demonstrating bidirectional pumping and high
60 flow-rates. Our solid-state stretchable pumps have no moving parts, are silent, produce no
61 vibration, and operate well when highly bent and even stretched, making them ideal candidates for
62 miniaturization and portability in soft systems.

63
64 The modular pumps we developed are compact (75 mm long \times 19 mm wide \times 1.3 mm thick with
65 a fluidic channel of dimensions 55 mm long \times 2 mm wide \times 0.5 mm thick), light-weight (1.0 g)
66 and are controlled simply by changing the applied voltage. The pump body material is PDMS
67 (Polydimethylsiloxane) in view of its low Young's modulus, high strain at rupture ($>100\%$), and
68 widespread use in microfluidics. We use established elastomer processing technologies which are
69 highly reproducible and can readily be scaled up for industrial production^{27–29}. The cross-section
70 and length of the channel, number of electrodes, and gap between them, can all be easily scaled up
71 or down thanks to our versatile fabrication methods. Extended Data Fig. 2 shows the details of the
72 fabrication process of the pumps, while Extended Data Fig. 3 shows the four generations of pumps
73 that we developed.

74 Numerous combinations of materials can be implemented for the pump body, electrode, and
75 dielectric liquid, subject to the requirement that the body and electrodes must be stretchable. We
76 focus on two versions that share the same channel geometry and interdigitated electrode design,
77 but with different electrode materials and operating liquids, to illustrate the dependency of pump
78 performance on materials. We refer to the two devices as the “C pump” and “Ag pump” with
79 Carbon- and Silver-based electrodes.

80
81 The C pump electrodes are a stretchable composite of carbon black and PDMS, patterned by laser
82 engraving; the fluid is Novec 7100 from 3M. The Ag pump uses a printed stretchable silver ink
83 (Chimet Ag 520 EI) electrodes, and Fluorinert FC-40 from 3M as the dielectric liquid. The Ag
84 devices offer much longer lifetime and higher pressure, but requiring higher voltages than the C
85 pumps. Fluorinert FC-40 is compatible with most elastomers, including PDMS, allowing reliable,
86 long-term operation of the pump. In contrast, Novec 7100 swells PDMS, but is widely used in rigid
87 EHD devices. Ag electrodes enable continuous pumping operation for many hours, while the
88 carbon electrodes have a limited lifetime of order 15 minutes. An advantage of the C pumps is a
89 minimum voltage for pumping that is roughly half that of Ag pumps (2.5 kV vs. 5 kV). However,
90 the Ag pumps can sustain roughly twice the voltage of the C pump (10 kV vs. 6 kV) and can thus
91 generate higher maximum pressure. For the C pump, we measured a generated pressure of over 7
92 kPa and a maximum flow-rate of over 100 $\mu\text{l/s}$ at 5.6 kV, compared to a maximum pressure of over
93 14 kPa at 10 kV for the Ag pump. The response time is under one second from zero to maximum
94 pressure for the C pump. The Ag pumps shows in general a slower response. Its performance can
95 be increased by a brief pre-conditioning step at high fields (20 kV/mm).

96

97 Figure 2 shows the results of both steady-state and transient characterization experiments. The very
98 low electrical current (1-20 μA) and low power (100 mW) allows powering the pumps by means
99 of miniature batteries and miniaturized DC converters (Extended Data Fig. 4). Flow-rate and
100 pressure values are high enough for macro-scale applications. Additionally, the modular pump
101 elements can be connected in series (Fig. 2F and Extended Data Fig. 5) to increase the output
102 pressure or in parallel to multiply the flow rate. Safe operation on the human body is enabled by
103 using only materials and liquids with very low toxicity and by limiting the electrical current to
104 values far below the human-safety threshold. The intrinsic compliance, low mass, and low power
105 consumption make the soft pumps an enabling tool for portable soft robotics and fluid-based
106 wearable devices. The key performance metrics of our stretchable pumps, including specific
107 pressure, specific flow-rate, and specific power consumption, are comparable to those of published
108 micropumps and commercial pumps, see Fig. 1c and Extended Data Table 1 which contains an
109 overview of pumps operating on a wide range of principles as reviewed in ^{20,30,31}.
110

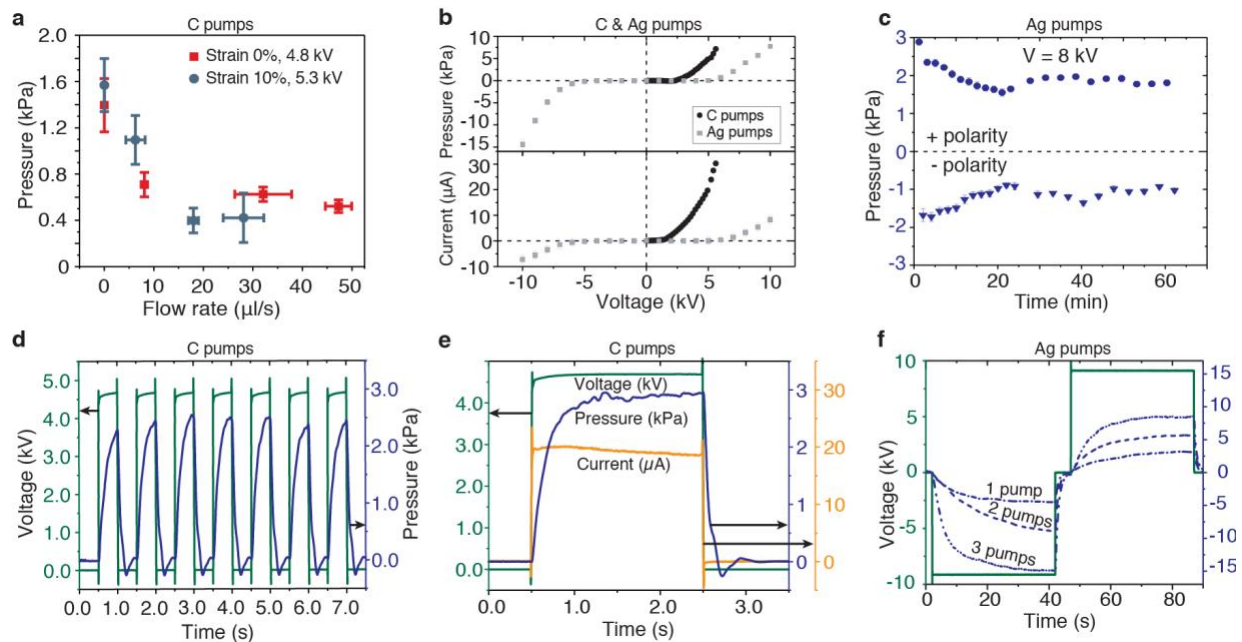


Fig. 2: Performance of the stretchable EHD pumps. **a**, Pressure vs. flow rate for the C pump at 0% and 10% strain. Error bars represent the standard deviation. The voltage was increased by 10% at 10% strain to keep the same electric field as at 0% strain. **b**, Pressure and electrical current vs. applied voltage, for zero flow-rate (the output valve is closed), for both C and Ag pumps. For the Ag pumps, the flow direction can be reversed by reversing the polarity of the applied voltage. **c**, Lifetime test on the Ag pumps, applying a $\pm 8 \text{ kV}$ square wave for one hour. **d**, Pressure generated by the C pump in response to a 1 Hz 0-5kV square wave. **e**, Transient response of the C pumps to a 4.5 kV voltage step, showing a pressure rise time of 0.4 s and a fall time of 0.14 s, both at 10% to 90% pressure. **f**, Pressure generated by three pumps connected in series, when 1, 2 or all the 3 pumps are activated. For the 1 pump and the 2 pumps curves, the data shown are the mean over three experiments, in order to include data from all three devices.

111

112 While the C and Ag pumps can both operate at strains of over 50%, we characterized the

113 performance of the C pumps at 0% and 10% applied strain (Fig. 2a) as these strain levels are typical

114 of many soft robotics or wearable applications. The simultaneous measurement of generated flow

115 rate and pressure provides the characteristic curve of the stretchable pumps (Fig. 2b), showing a

116 sub-linear decrease of the pressure as the flow-rate is increased. Performance is nearly unchanged

117 at 10% strain for constant applied electric field. The planar and symmetric electrode design allow

118 the generation of flow in both directions, based on the direction of the applied electric field, as

119 shown in Fig. 2b for the Ag pump, whose pumping direction can be repeatedly reversed. The C

120 pumps can also pump in either direction, but unlike the Ag pumps, the C pumps only operate in
121 the direction in which the field was applied at first operation. Fig. 2c shows a lifetime test of the
122 Ag pump, driven by a bipolar ± 8 kV square wave. The period of the square wave is 120 s for the
123 first 25 min and 240 s in the following 35 min. The pumps are undamaged after this experiment,
124 thanks to the very good compatibility between PDMS, the Ag electrodes and the FC-40 dielectric
125 liquid. Fig. 2d-e show the transient response of the C pumps to a 1 Hz unipolar square wave and a
126 5 kV voltage step. The pressure-voltage response is stable and repeatable. Figure 2f demonstrates
127 pump modularity: three pumps are connected in series (Extended Data Fig. 5) and total pressure is
128 measured when one, two or all the three pumps are activated. The generated pressure scales with
129 the number of active pumps.

130 There is a large parameter space of electrode configurations and channels geometries that could be
131 explored to further increase performance, see Methods section and Extended Data Fig. 1. The
132 differences between C and Ag pumps indicate that electrode materials and fluid choice play an
133 important role, and offer an avenue to further improve pressure and flow rate.

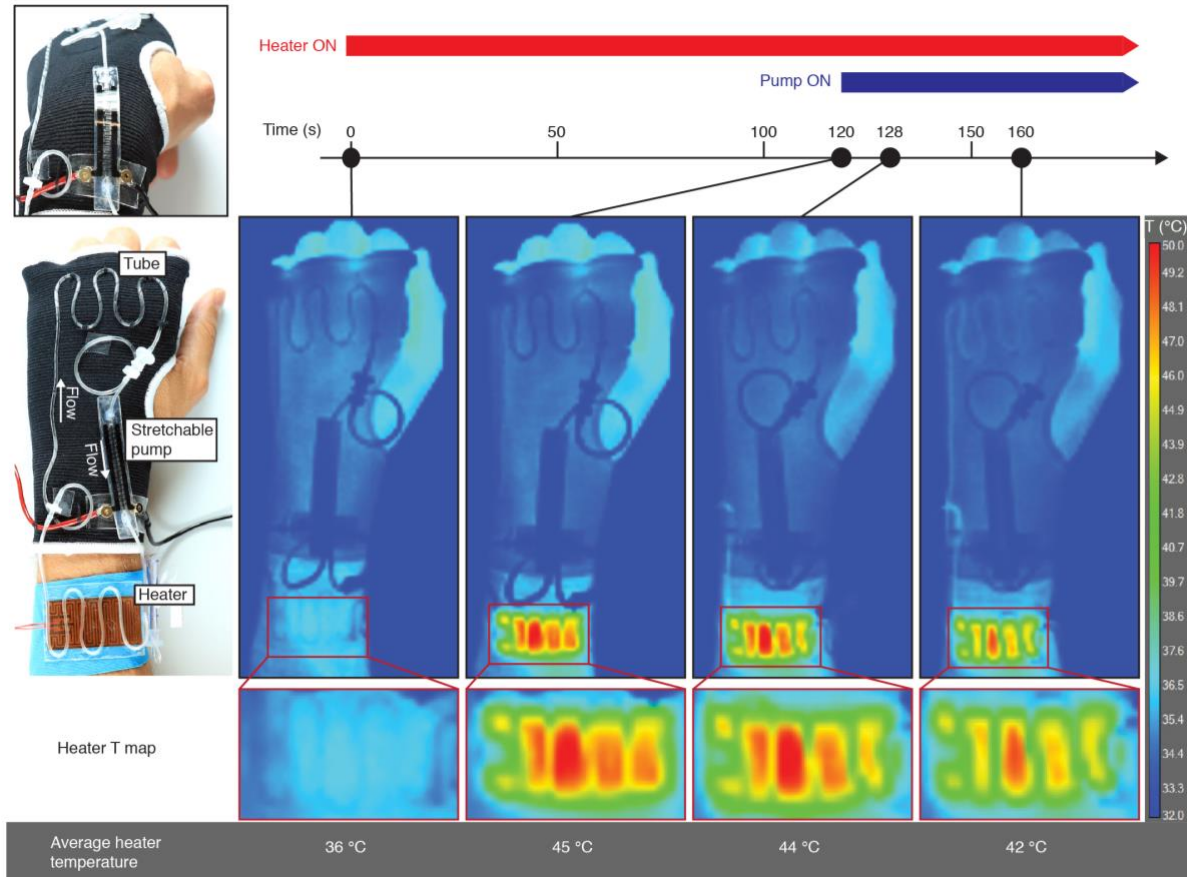


Fig. 3: The stretchable pump is embedded in a textile glove for on-body thermal regulation. The closed loop fluidic circuit consists of the pump and a serpentine flexible tube sewn into the textile glove (the “cold” side), and of a serpentine flexible tube bonded to a flexible heater (the “hot” side). The wearer can easily flex his wrist while the pump is operating. The pump circulates the fluid from the heater to the glove and then back on the opposite side. The colors in the IR images correspond to a temperature map, see colorbar on the far right. The leftmost IR image shows the initial condition when both heater and pump are off. For the second IR image, the heater is on and the pump is off: the temperature at the heater is significantly higher than at the arm. The third IR picture is taken at few seconds after the pump is activated. One can see the cold liquid entering the “hot” circuit from the right tube and the heat being transported away from the left tube. The rightmost IR image shows that the temperature of the heater is significantly decreased after 40 s of fluid circulation. The unchanged temperature of the soft pump confirms its negligible heat generation. Supplementary Video 3 shows the device in action.

135 We illustrate the broad applicability of the stretchable pumps by demonstrating both a wearable
136 and a soft robotics scenario. In the wearable scenario, the pump is integrated in a textile glove to
137 actively circulate fluid to transport heat between regions on the body (Fig. 3). In the soft robotics
138 scenario, we demonstrate a self-contained fluidic actuator where the pump is embedded in the soft
139 bending structure to move the fluid between two chambers, resulting in large actuation without
140 external fluidic connections (Fig. 4).

141 For the wearable demonstrator for temperature control (Fig. 3), the pump is integrated in a textile
142 glove and circulates the dielectric fluid from a hot zone, consisting of a membrane heater, to a
143 cooling tubing embedded in the glove. We monitor the temperature of the system using an infrared
144 (IR) camera, which showed that the temperature of the heater was significantly decreased by fluid
145 circulation and that the soft pump did not heat the liquid, thanks to the pump's low power
146 consumption.

147 The heater in this experiment can represent for example overheating following intense physical
148 activity. For a temperature difference $\Delta T = 6$ K and a flow rate $Q = 100$ $\mu\text{l/s}$, we can estimate a
149 heat transport ability of 1.1 W, one order of magnitude higher than the power consumption of the
150 pump (~ 0.1 W), showing its effectiveness as a wearable thermal regulation device. The
151 experimental results shown in Fig. 3 confirm this estimation, as the pump transports the heat away
152 from an overheated body area to the periphery (Supplementary Video 3). More information on the
153 thermal regulation experiments can be found in the Methods section. Thanks to its small size,
154 compliance and low-weight, the stretchable pump does not interfere with the physical movements,
155 paving the way for wearable fluidic circuits for thermal regulation constituted by multiple pumps
156 which could be integrated in everyday clothing, sportswear or wearable protections for severe
157 environments.

158

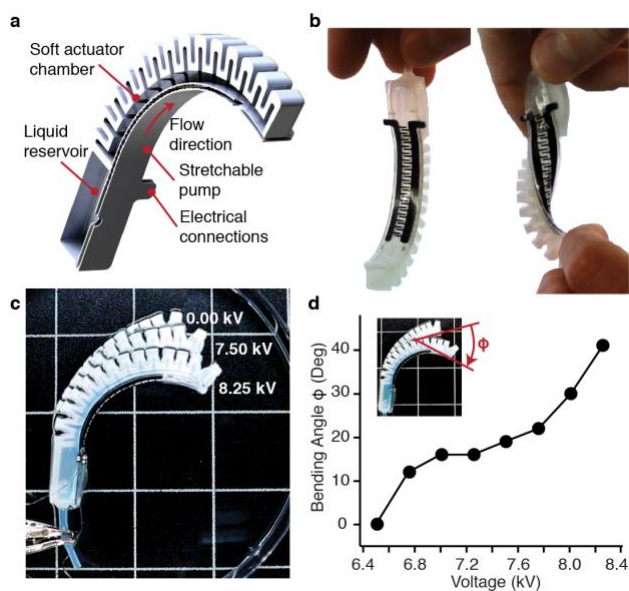


Fig. 4: Fluidic muscles obtained by bonding a stretchable pump to a bending fluidic actuator. **a**, Schematic longitudinal cross section of the fluidic muscle, showing the main components. The inlet of the pump is connected to a small reservoir at the back of the actuator, while the outlet is connected to the bellows-shaped bending chamber. **b**, The entire actuator is soft and can be easily deformed. **c**, Once pre-filled with dielectric liquid, the actuator does not have any external tubing. It bends when a voltage is applied: the soft pump moves the liquid from the reservoir to the bending chamber, producing its deformation. **d**, Measured bending angle as a function of the applied voltage. Supplementary Video 4 shows the fluidic muscle in action.

159
 160 We then considered the integration of the stretchable pumps in fluidic actuators, which are often
 161 used in combination with conventional rigid pumps or compressors. Figure 4 shows a fluidic

162 muscle composed of a bending fluidic actuator⁷ with a stretchable pump embedded in its bottom
163 layer. The pump pushes liquid from a small reservoir in the back of the actuator to a bellows-shaped
164 chamber, whose inflation causes bending of the actuator. When the voltage is applied, the actuator
165 bends by over 40° relative to its rest position (Fig. 4c-d and Supplementary Video 4). Figure 4d
166 shows the fluidic muscle's angle vs. voltage curve, whose shape results from a combination of the
167 nonlinear response of bending fluidic actuators and that of the soft pump (Fig. 2c). When the
168 voltage is removed, the fluidic muscle returns to its initial position thanks to the restoring elastic
169 forces of the chamber. Such actuators are promising building block for the next generation of soft
170 robots, combining the robustness, large deformation and versatility of fluidic actuators with the
171 portability of an integrated system that does not require external compressors.

172

173 **METHODS**

174

175 **ElectroHydroDynamics (EHD) pumping principle**

176 EHD pumping refers to the acceleration of a fluid by means of an electric field¹⁹. In this work, we
177 explored two EHD pumping mechanisms.

178 The first mechanism (Extended Data Fig. 1a) is called conduction pumping and relies on the
179 formation of heterocharge layers in the proximity of the electrodes²¹. Heterocharge layers are non-
180 equilibrium charged layers that form when the electric field exceeds a certain threshold (5 –
181 6 V/ μm) due to ion generation not balanced by recombination. The charges in these layers are of
182 opposite sign to that of the adjacent electrode, thus they are electrostatically pulled towards the
183 electrode, where they discharge. The movement of ions, which drags the neutral liquid molecules
184 and thus generates pumping, is identical at the anode and at the cathode. As a consequence, to
185 obtain global flow (i.e., not simply local recirculation) the electrodes surface must be oriented such
186 that the direction normal to the electrodes has a non-zero component oriented in the direction of
187 the desired flow. The flow direction is therefore determined by the design of the electrodes and not
188 by the field polarity. This conduction pumping mechanism consists of an array of inclined
189 capacitors obtained by overlapping symmetrical electrodes on an inclined channel, as shown in
190 Extended Data Fig. 1a.

191 The second mechanism (Extended Data Fig. 1b) is called charge injection and is based on field
192 emission^{20,22}. When the electric field is high enough, electrons can overcome the energy barrier
193 and directly tunnel from the cathode surface into the dielectric liquid. The ions thus formed are
194 accelerated by the electrophoretic force until they discharge at the anode. The use of dielectric
195 liquids with highly electronegative molecules (e.g., fluorine-based liquids) ensures that the energy
196 barrier for field emission to occur at the cathode is significantly lower than at the anode. This
197 mechanism can create net flow with a planar electrodes configuration and a DC electric field. The

198 flow direction can be inverted by inverting the polarity of the electric field. Extended Data Fig. 1b
199 shows the design of the soft pump based on injection pumping, consisting of two overlapped sets
200 of interdigitated electrodes.

201 In both mechanisms, once one has exceeded the electric field threshold needed for the phenomenon
202 to occur, the pumping pressure Δp grows with the square of the electric field and linearly with the
203 dielectric constant of the liquid: $\Delta p = k_p \epsilon E^2$, where k_p is a constant depending on the pump
204 geometry. The generated flow-rate Q has a more complicated relation; it generally depends on the
205 electric field squared and on the fourth power of the channel size D : $Q = k_Q \epsilon E^2 D^4$. The direction
206 of the flow is opposite to the direction of the electric field for charge injection, while it depends
207 only on the geometry of the electrodes for conduction pumping.

208 One has a great deal of design freedom for the EHD electrode configurations. For the interdigitated
209 case, one can reduce the inter-electrode distance g to simultaneously lower the drive voltage for a
210 given electric field and to increase the number of electrode pairs (hence pressure) in a given channel
211 length. How the inter-electrode gap influences pressure and flow rate is non-trivial: a smaller gap
212 spacing leads to electric field lines that penetrate less far into the channel, thus dragging ions along
213 a thinner sheath. Increasing the width of the electrodes will proportionally increase flow rate.
214 Scaling down ever further leads to lower voltages but creates a flow only very near to the wall,
215 with much higher friction losses. We propose that a gap of order channel thickness is a reasonable
216 starting point.

217 Dielectric fluids for EHD pumping must have low electrical conductivity ($<10^{-7}$ S/m) and high
218 electrical breakdown strength to enable high pumping pressure. Of the different liquids one can
219 consider, Novec 7100 and Fluorinert FC40 both have excellent dielectric strength, with nominal
220 breakdown voltages of 10-16 kV and > 18 kV for 1 mm gaps, respectively. The boiling points of
221 Novec 7100 and Fluorinert FC40 are 61 °C and 155 °C, making them well-suited for room

222 temperature operation. Both fluids have very low toxicity, zero ozone depletion potential, no flash
223 point and are nonflammable.

224

225 **Stretchable pumps: four generations**

226 We designed and developed four generations of stretchable pumps (Extended Data Fig. 3). The
227 circuit of the first generation (“inclined 1”, see Extended Data Fig. 1a) consists of a set of 5 inclined
228 capacitors (corresponding to 10 electrode units) separated by a 1 mm gap. It operates according to
229 EHD conduction pumping principles. The second generation (inclined 2) is a scaled down version
230 of the first one with half the channel size, half the electrode gap, and 43 inclined capacitors (86
231 electrode units).

232 The third generation (C pump) relies on the charge injection mechanism (Extended Data Fig. 1b)
233 and thus presents a different electrode layout: two series of 17 interdigitated electrodes facing each
234 other (68 electrode units). The fourth generation (Ag pump) has the same geometry as the third one
235 but the electrode material has been replaced by a commercial silver ink. The reason for this
236 materials change is the degradation observed in the performance of carbon-based electrodes, which
237 is completely solved by using silver particles as a conductive material.

238 The inclined design presents lower pumping performance for the same applied voltage compared
239 to the interdigitated design, as shown in Extended Data Fig. 3. Additionally, the interdigitated
240 design allows pumping in either direction, based on the polarity of the applied voltage, while the
241 inclined design always generates flow according to the gradient in the electric field (from the larger
242 gap side to smaller gap side). However, the conduction pumping mechanism is less subject to
243 electrodes deterioration than the charge injection used in the interdigitated design^{19,21,22}. Another
244 advantage of the inclined design over the interdigitated one is robustness to minor electrical
245 breakdown events. In the inclined design, the short-circuit path between electrodes with opposite

246 polarity is always through the dielectric liquid, so permanent short circuits do not form, as in
247 HASEL actuators¹². On the contrary, in the interdigitated design, conductive paths can form on the
248 PDMS substrate rather than through the liquid, preventing the healing of the device.

249 A comparison between the inclined 1 and inclined 2 designs shows the scalability of the stretchable
250 pumps both in terms of channel size and electrodes spacing. By varying the channel height, which
251 in this configuration corresponds to the gap between the electrode pairs (Extended Data Fig. 1a),
252 we change the electric field at a given voltage. As a consequence, the response of the inclined 1
253 pump is shifted to double the voltages of the inclined 2, as we would expect since the EHD
254 phenomenon depends on the value of the electric field. We can also observe a direct proportionality
255 between the number of electrode pairs and the generated pressure.

256

257 **Materials and Fabrication**

258 The stretchable pumps are composed of two electrode layers that sandwich a channel layer. The
259 Polydimethylsiloxane (PDMS) used for the pump body is Dow Corning Sylgard 184. The electrode
260 layers are symmetric and are patterned on a 0.4 mm thick PDMS backing. The electrode material
261 for the C pumps is composed of carbon particles dispersed in a soft PDMS matrix³² (Silbione LSR
262 4305), while for the Ag pumps the electrode is printed using a commercially-available stretchable
263 silver ink (Chimet Ag 520 EI) using a laser-engraved Mylar (BoPET, Biaxially-oriented
264 polyethylene terephthalate) mask. The channel layer consists of a laser-cut PDMS membrane,
265 whose thickness determines the height of the channel (1.0 mm or 0.5 mm in the devices we
266 developed). The layers are bonded using a silicone adhesive film (AR Clear 8932EE, Adhesives
267 Research), which is laminated on the channel layer before the laser cutting process. Extended Data
268 Fig. 2 shows the details of the fabrication process. The dielectric liquids used for the stretchable

269 pumps are fluorinated solvents: 3M Novec 7100, methoxy-nonafluorobutane ($C_4F_9OCH_3$) for the
270 C pumps, and 3M Fluorinert FC-40 ($C_{10}HF_{22}N$) for the Ag pumps.

271

272 **Characterization experiments**

273 Pressure and flow-rate measurements were performed using the pumps in a closed loop with a
274 variable-opening valve to control the fluidic impedance. The pumps were powered using power
275 supplies based on the Peta-Pico-Voltron³³ (<https://petapicovoltron.com/>) open source HV supply
276 for voltages up to 5 kV, and using an EMCO regulated CB101 up to 10 kV. The applied voltage,
277 electrical current, pressure and flow-rate were simultaneously recorded.

278

279 The Ag devices operate stably in air with no special pre-treatment: we routinely operated the Ag
280 pumps in lab ambient for several hours. For the C pumps however, most characterization
281 experiments were conducted with the stretchable pumps submerged in the same dielectric liquid
282 used for pumping (3M Novec 7100), as operating in liquid allows for long-term testing for the C
283 pumps. PDMS is permeable to, and swells in, Novec 7100; operating in air eventually results in
284 gas bubbles inside the channel. Soaking the device in Novec 7100 temporarily prevented gas
285 formation and allowed reliable operation in air for up to 15 min.

286 The thermal regulation and soft robotic actuator experiments were carried with C pumps in air after
287 soaking the pump in the dielectric liquid for 10-15 min.

288

289 **Heart-shaped balloon**

290 The heart-shaped balloon consists of two separate fluidic chambers (ventricles). It is manufactured
291 by mold casting a soft silicone rubber (Smooth-on Ecoflex 0030) in a CNC-machined plastic mold
292 and then gluing this molded body to a 100 μ m thick membrane made with the same silicone. Each

293 side of a stretchable pump is connected to one of the two ventricles of the balloon using small vinyl
294 tubes (1.2 mm ID). Before each experiment, the circuit is pre-filled with dielectric liquid (FC-40)
295 and most of the air is removed. The voltage is applied to the pump using a battery-driven high-
296 voltage power supply (Extended Data Fig. 4). Based on the polarity of the applied voltage, the
297 pump moves the liquid from the left ventricle to the right one or vice-versa (Fig. 1d, Supplementary
298 Video 2). In this experiment, we used a modified version of the Ag pump, where the gap between
299 the interdigitated electrodes has been reduced from 0.5 mm to 0.4 mm to increase the electric field
300 for the same applied voltage and comply with the maximum 6 kV output of the battery-driven
301 power supply.

302

303 **Thermal regulation on a smart glove**

304 In this experiment, the fluid circulation driven by a stretchable pump transfers heat between a hot
305 area and a cold one. To a first approximation, the rate of heat transfer H in a fluidic heat exchanger
306 is proportional to the flow-rate Q , according to the equation $H = Q\rho c_p \Delta T$, where $c_p =$
307 1183 J/kg/K is the specific heat of our working fluid (Novec 7100), $\rho = 1510 \text{ kg/m}^3$ its density
308 and ΔT the temperature difference between the inlet and the outlet of the exchanger. The rate of
309 heat transfer H , measured in watts, represents the amount of thermal power that can be transported
310 by the fluid.

311 The hot area in our set-up is represented by a flexible joule heater (MINCO polyimide thermofoil
312 heater) while the cold one by a serpentine sewed in a textile glove, where the heat can be dissipated
313 by natural air convection. The closed-loop fluidic circuit is filled with dielectric liquid and air
314 bubbles are removed before activating the pump. We apply a constant voltage of 9V on the heater,
315 leading to a thermal power of 1.2 W. The temperature map is acquired using an IR camera (FLIR
316 A15, 50 mK thermal sensitivity). The emissivity is set to a constant value of 0.98, given the very

317 similar values of emissivity of all the materials involved in the set-up (i.e., human skin, elastomers,
318 plastic foils).

319

320 **Soft robotic actuator**

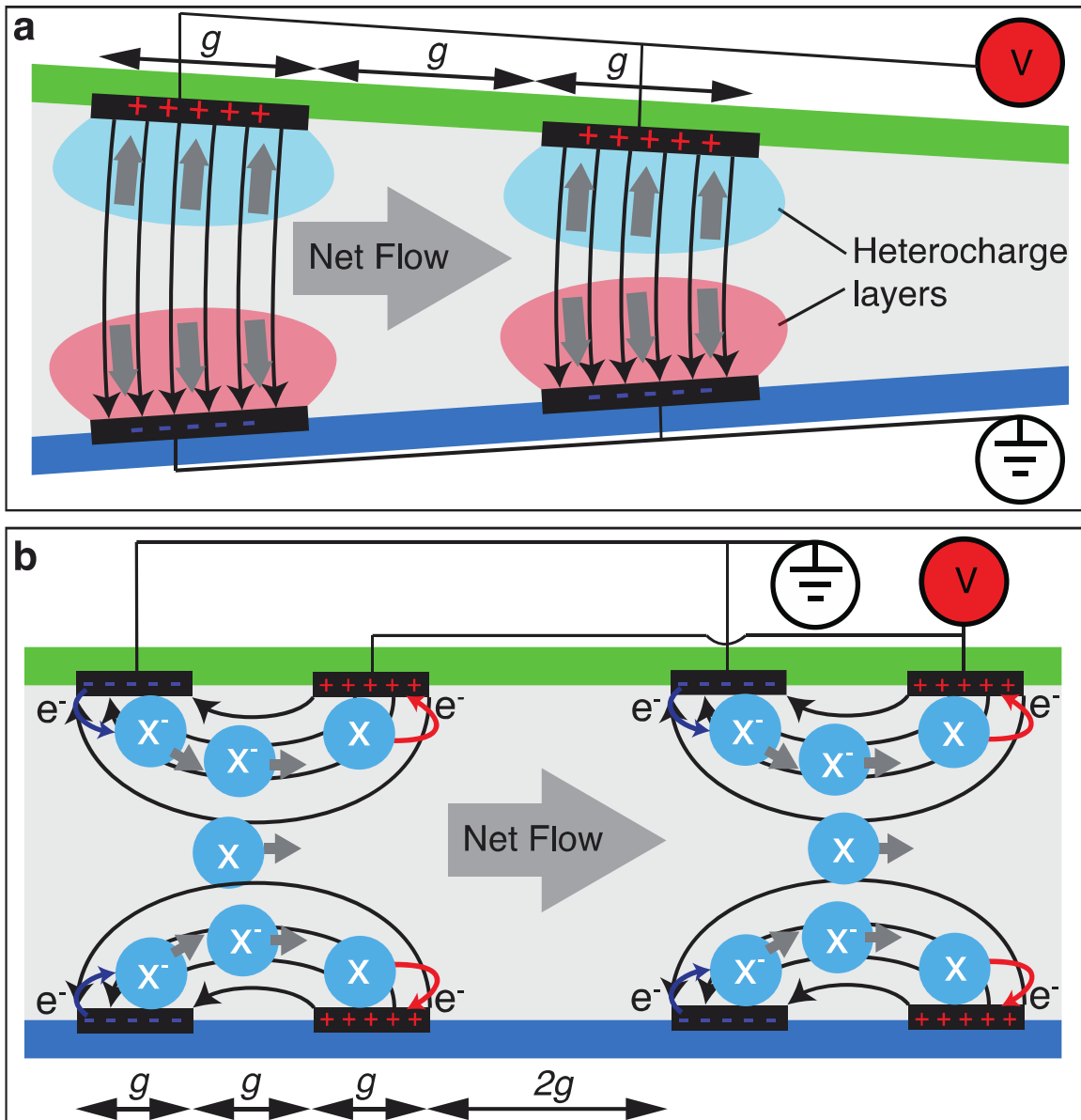
321 The bending fluidic actuator is manufactured by mold casting a soft silicone rubber (Smooth-on
322 Ecoflex 0030) in a 3D printed mold⁷. Pump and actuator are bonded together, fluidically connected
323 and sealed using a silicone glue (Wacker Silpuran 4200). The experiment is conducted with the
324 soft actuator lying on a horizontal plane lubricated with Novec 7100 to prevent stiction. Before
325 starting the experiment, the actuator is filled with dielectric liquid using the tube in its back. Air
326 bubbles are evacuated using gravity. The actuator reservoir is filled with dielectric liquid and the
327 actuators takes a curved shape at rest due to the liquid pressure. This pressure causes the pump
328 channel to expand slightly, resulting in slightly higher pump working voltages compared to the
329 uninflated case. The bending is recorded with a camera and the angle computed using Kinovea
330 software for image analysis.

331

332 **Data availability**

333 All data are available from the corresponding authors upon reasonable request.

334

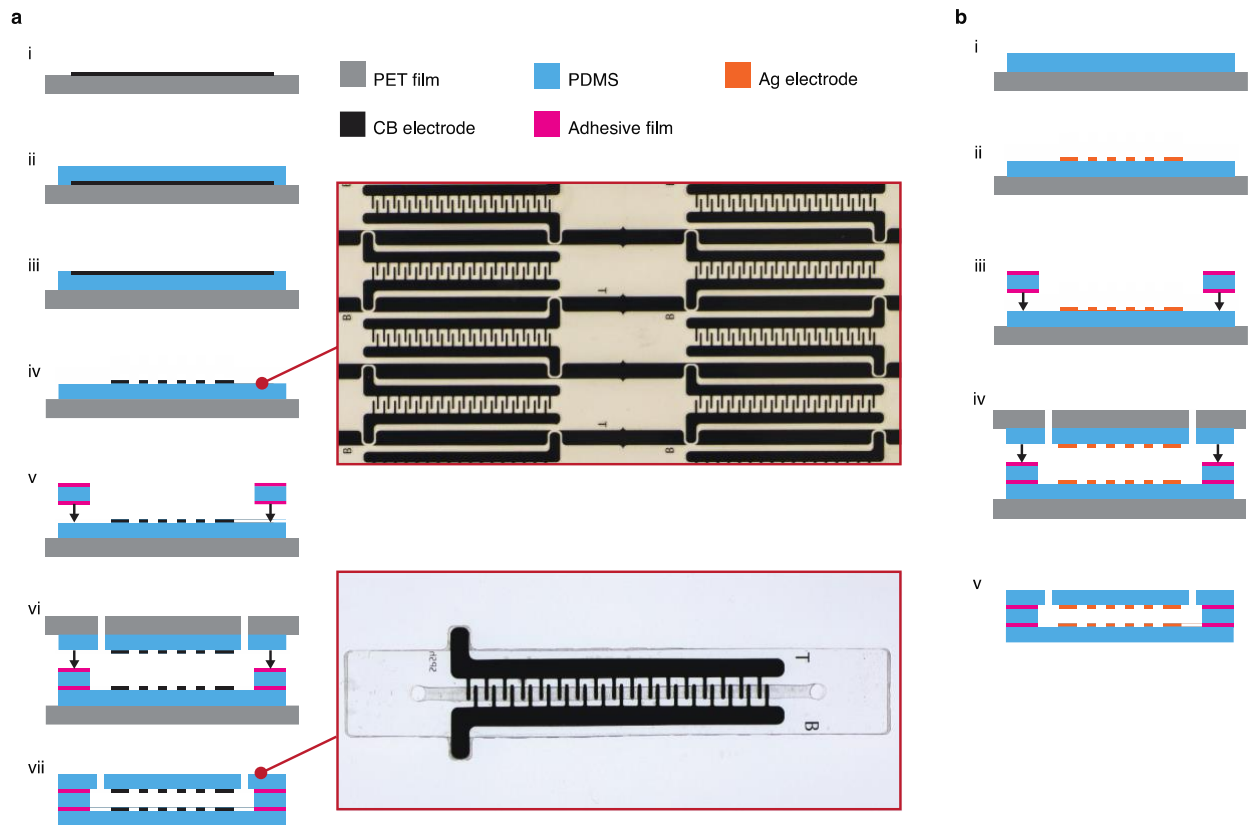


335

336 **Extended Data Figure 1: The two different electrode geometries and corresponding**
 337 **ElectroHydroDynamic (EHD) mechanisms used in this work.**

338 **a**, Conduction pumping, with inclined capacitors. Heterocharge layers form in the proximity of the
 339 electrodes. These layers are characterized by a higher concentration of ions of opposite polarity
 340 with respect to the opposing electrode. As a consequence, these ions are attracted to the opposite
 341 electrode, where they discharge. The inclined capacitors geometry allows net flow thanks to the in-
 342 flow component of the electric field in proximity of the electrodes surface. **b**, Charge injection,
 343 with interdigitated electrodes. When the electric field is high enough to overcome the energy
 344 barrier, field emission takes place, with electrons tunneling from the cathode into the dielectric
 345 liquid. The generated ions are accelerated by the electric field until they discharge at the anode,
 346 transferring momentum to neutral liquid molecules along the way.

347

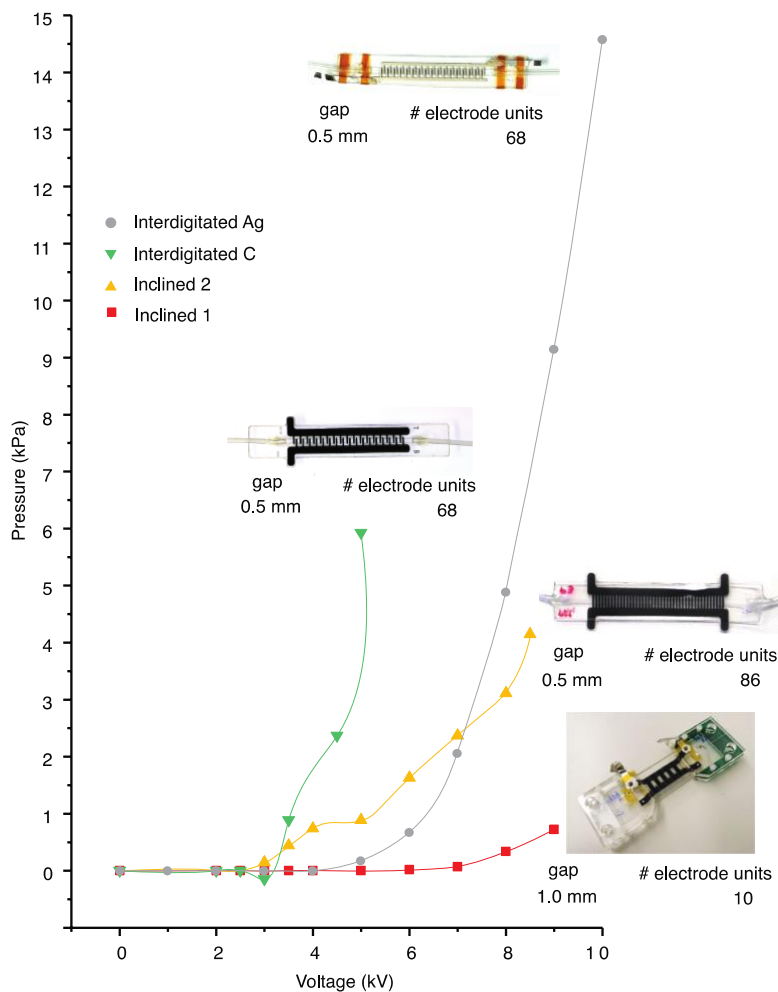


348

349 **Extended Data Figure 2: Fabrication process for the stretchable pumps using the**
 350 **interdigitated design.**

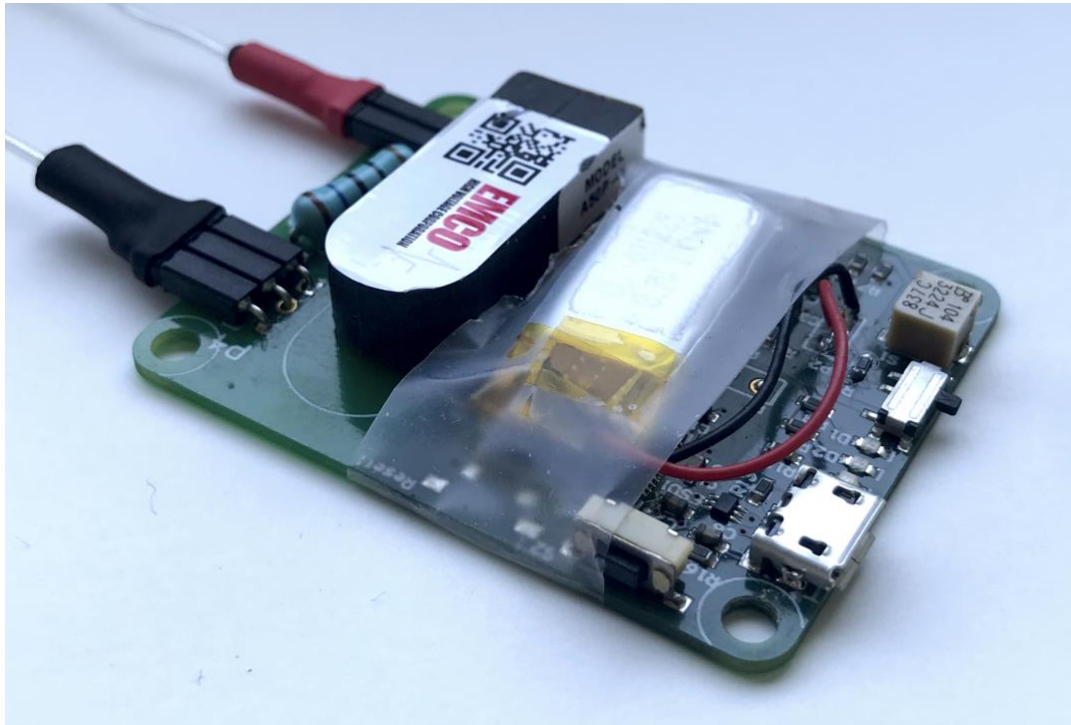
351 **a**, Fabrication process of the C pump. (i) The fabrication of the electrode layers starts by blade
 352 casting a carbon-based electrode membrane with a thickness of 30 μm on a PET support, which is
 353 then cured at 80 $^{\circ}\text{C}$ for 2 h. (ii) A 400 μm PDMS membrane is casted on the top of the electrode
 354 and cured at 80 $^{\circ}\text{C}$ for 1 h. (iii) The sample is turned over in order to expose the electrode
 355 membrane, (iv) which is then processed by laser engraving to define the interdigitated pattern. This
 356 process allows the manufacturing of many samples in parallel (up to 24 samples with our
 357 equipment at EPFL-LMTS). (v) The channel layer, consisting of a 500 μm thick laser-cut PDMS
 358 membrane, is bonded on the bottom electrode layer using a silicone adhesive film. (vi) The top
 359 electrode layer, having two laser-cut holes for fluidic connection, is finally bonded on the top of
 360 the channel layer. (vii) The PET supports are removed and the C stretchable pumps are ready to
 361 use. **b**, Fabrication process of the Ag pump. (i) The fabrication starts by blade casting and curing
 362 (80 $^{\circ}\text{C}$, 1h) a 400 μm PDMS membrane. (ii) On the PDMS, a silver-based stretchable ink is printed
 363 through a 23 μm thick Mylar mask and cured at 80 $^{\circ}\text{C}$ for 3 h. (iii) After removing the mask, the
 364 bottom electrode layer is bonded to the 500 μm thick channel layer using a silicone adhesive film.
 365 (iv) The top electrode layer, having two laser-cut holes for fluidic connection, is finally bonded on
 366 the top of the channel layer. (v) The PET supports are removed and the Ag stretchable pumps are
 367 ready to use.

368
 369



370
 371 **Extended Data Figure 3: Four generations of stretchable pumps plotting generated**
 372 **pressure vs. applied voltage.**
 373 The “inclined 1” and “inclined 2” generations have inclined capacitors as the electrode
 374 configuration. “inclined 2” is a scaled version of “inclined 1”, with half the channel size, half the
 375 gap between opposite electrodes, and 8.6 times more electrode pairs. The interdigitated
 376 generations have the same channel size and gap between opposite electrodes as “inclined 2”, but
 377 use interdigitated electrodes rather than inclined capacitors. The C version has laser-engraved
 378 carbon-silicone composite electrodes and uses 3M Novec 7100 as the dielectric fluid, while the
 379 Ag version has mask-printed silver-based electrodes and uses 3M Fluorinert FC-40 as the
 380 dielectric fluid. The Ag devices can sustain higher fields than the C devices thanks to the
 381 different dielectric liquid and to the different electrode fabrication method.
 382

383



384

385 **Extended Data Figure 4: A 5 kV programmable power supply weighing 16 g, including Li-**
386 **ion battery.**

387 This custom-made power supply is based on an EMCO DC-DC converter from XP-power
388 (<https://www.xppower.com/Product/A-Series/>) and includes a microcontroller to program the
389 output. Dimensions are 5 cm × 4 cm × 0.8 cm. In this work we also used a 6 kV, 20 g version.

390



392

393 Extended Data Figure 5: Three stretchable pumps connected in series.

394 The data shown in Fig. 2f were taken using these three pumps connected in series to increase
395 pressure. Alternatively, pumps could be connected in parallel for higher flow rate. Each pump is
396 7.5 cm long.

397

398 **Concise overview of miniature pump performance**

399
400 Table 1 below compares performance of pumps based on a broad range of physical principles, as
401 reviewed in 20,30,31. Some numbers, pump overall volume in particular, are approximate because
402 authors include different elements when reporting pump dimensions, in part due the large range of
403 possible actuation methods.

404 Our stretchable pump significantly surpasses all reported soft pumps in both specific pressure and
405 specific flow rate.

406 Amongst published soft pumps, combustion-driven pumps provide the highest absolute pressure
407 and flow rates, but require a source of combustible gas, an ignition system, and a design that can
408 tolerate the high combustion temperatures and pressure bursts. Those pumps can be challenging to
409 regulate and are mostly adapted to generate explosive motion such as for jumping robots.

410 Electroosmotic pumps are in principle well-suited to fabrication in a stretchable format given their
411 simple structure. The one reported stretchable device is fabricated with extremely small
412 micromachined channels, leading to very low flow rates, far too small for soft robotics or wearable
413 applications. Pneumatic actuation allows for ready use of soft materials, but the need for an external
414 source of compressed air is impractical for the applications we report in this paper.

415
416

Extended Data Table 1: Pump performance comparison

Category	Reference	Pumping Principle	Approximate Size (cm ³) [*]	Max. Power Consumption (W)	Max. pressure (kPa)	Max. Flow Rate (ml/min)	Max. Power Consumption / Size (× 10 kW/m ³)	Pressure / Size (GPa/m ³)	Flow Rate Size (×10 ³ l/min/)
Stretchable pumps	This study	Electrohydrodynamic	1.17	0.17	14	6.0	14.5	12	5.13
Commercial pumps	High performance miniature pump (MGD 1000S) ³⁴	Electromagnetic	58.6	30	800	500	51.2	13.7	8.5
	Off-the-shelf compressor (McMaster STPAC) ³⁵	Electromagnetic	75500	1200	1034	42500	1.59	0.01	0.56
Micropumps [†]	36	Piezoelectric	0.26	N/A	74	1.1	N/A	284	4.2
	37	Piezoelectric	1.98	0.4	0.52	0.04	20.2	0.26	0.02
	38	Electromagnetic	3.5	0.17	8	9.5	4.86	2.29	2.71
	39	Electromagnetic	50.6	N/A	25.5	0.14	N/A	0.5	0.003
	40	Electrohydrodynamic	0.01 [‡]	N/A	1.75	14	N/A	175	1400
	41	Electrohydrodynamic	0.09 [‡]	0.35	0.25	0.04	389	2.78	0.44
	42	Electroosmotic	0.04 [‡]	0.88	10000	0.002	2200	250000	0.05
	43	Electroosmotic	9	0.002	33	0.02	0.02	3.67	0.002
	44	Electrostatic	0.1	N/A	29	0.16	N/A	290	1.6
	45	Piezoelectric	0.26	N/A	74	1.1	N/A	284	4.2
	46	Magneto-hydrodynamic	2.03	N/A	0.75	0.7	N/A	0.37	0.25
	47	Ionic	0.8	N/A	0.17	0.005	N/A	0.21	0.001
	48	Thermo-pneumatic	3	N/A	5.1	0.03	N/A	1.7	0.01
	49	Phase change	0.07	N/A	0.1	0.006	N/A	1.43	0.086
	50	Thermo-pneumatic	0.004 [‡]	3.4	0.49	0.01	85000	123	2.5
	51	Pneumatic	6	N/A	0.44	0.09	N/A	0.07	0.15
Pumps using soft or flexible materials	52	Thermo-pneumatic	11	N/A	3.5	0.02	N/A	0.32	0.002
	53	Electroosmotic	0.01 [‡]	N/A	0.01	0.001	N/A	1	0.1
	54	Combustion	49	N/A	60	40	N/A	1.22	0.82
	55	Pneumatic	500 (estimated from photo)	N/A	20	430	N/A	0.04	0.86
	56	Combustion	314	N/A	130	240	N/A	0.41	0.76

^{*} Volume based on data in paper, photographs/figures. We attempted to include the same key components in each pump for a fair comparison, despite important differences in fabrication methods and in operating principles.

[†] Reference selected from review articles 20,30,31. Some numbers differ from review article following analysis of the papers.

[‡] Channel or chamber dimensions, no data available on full pump.

418 **REFERENCES**

- 419
- 420 1. Rus, D. & Tolley, M. T. Design, fabrication and control of soft robots. *Nature* **521**, 467–475 (2015).
- 421 2. Laschi, C., Mazzolai, B. & Cianchetti, M. Soft robotics: Technologies and systems pushing the boundaries of
- 422 robot abilities. *Science Robotics* **1**, (2016).
- 423 3. Amjadi, M., Kyung, K.-U., Park, I. & Sitti, M. Stretchable, Skin-Mountable, and Wearable Strain Sensors and
- 424 Their Potential Applications: A Review. *Advanced Functional Materials* **26**, 1678–1698 (2016).
- 425 4. Hines, L., Petersen, K., Lum, G. Z. & Sitti, M. Soft Actuators for Small-Scale Robotics. *Advanced Materials* **29**,
- 426 1603483 (2017).
- 427 5. Suzumori, K., Iikura, S. & Tanaka, H. Development of flexible microactuator and its applications to robotic
- 428 mechanisms. in *1991 IEEE International Conference on Robotics and Automation Proceedings* 1622–1627
- 429 vol.2 (1991).
- 430 6. Suzumori, K., Wada, A. & Wakimoto, S. New mobile pressure control system for pneumatic actuators, using
- 431 reversible chemical reactions of water. *Sensors and Actuators, A: Physical* **201**, 148–153 (2013).
- 432 7. Polygerinos, P. *et al.* Soft Robotics: Review of Fluid-Driven Intrinsically Soft Devices; Manufacturing, Sensing,
- 433 Control, and Applications in Human-Robot Interaction. *Advanced Engineering Materials* **19**, 1700016 (2017).
- 434 8. Shintake, J., Cacucciolo, V., Floreano, D. & Shea, H. Soft Robotic Grippers. *Advanced Materials* **30**, 1707035
- 435 (2018).
- 436 9. Keplinger, C. *et al.* Stretchable, Transparent, Ionic Conductors. *Science* **341**, 984–987 (2013).
- 437 10. Viry, L. *et al.* Flexible Three-Axial Force Sensor for Soft and Highly Sensitive Artificial Touch. *Advanced*
- 438 *Materials* **26**, 2659–2664 (2014).
- 439 11. Rosset, S. & Shea, H. R. Small, fast, and tough: Shrinking down integrated elastomer transducers. *Applied*
- 440 *Physics Reviews* **3**, 031105 (2016).
- 441 12. Acome, E. *et al.* Hydraulically amplified self-healing electrostatic actuators with muscle-like performance.
- 442 *Science* **359**, 61–65 (2018).
- 443 13. Dong, L., Agarwal, A. K., Beebe, D. J. & Jiang, H. Adaptive liquid microlenses activated by stimuli-responsive
- 444 hydrogels. *Nature* **442**, 551–554 (2006).
- 445 14. Rossiter, J., Takashima, K., Scarpa, F., Walters, P. & Mukai, T. Shape memory polymer hexachiral auxetic
- 446 structures with tunable stiffness. *Smart Mater. Struct.* **23**, 045007 (2014).

- 447 15. Majidi, C., Kramer, R. & Wood, R. J. A non-differential elastomer curvature sensor for softer-than-skin
448 electronics. *Smart Mater. Struct.* **20**, 105017 (2011).
- 449 16. Cooper, C. B. *et al.* Stretchable Capacitive Sensors of Torsion, Strain, and Touch Using Double Helix Liquid
450 Metal Fibers. *Advanced Functional Materials* **27**, 1605630 (2017).
- 451 17. Pan, C. *et al.* Visually Imperceptible Liquid-Metal Circuits for Transparent, Stretchable Electronics with Direct
452 Laser Writing. *Advanced Materials* **30**, 1706937 (2018).
- 453 18. Besse, N., Rosset, S., Zarate, J. J. & Shea, H. Flexible Active Skin: Large Reconfigurable Arrays of Individually
454 Addressed Shape Memory Polymer Actuators. *Advanced Materials Technologies* **2**, 1700102 (2017).
- 455 19. Ramos, A. *Electrokinetics and Electrohydrodynamics in Microsystems*. (Springer Vienna, 2011).
- 456 20. Iverson, B. D. & Garimella, S. V. Recent advances in microscale pumping technologies: A review and
457 evaluation. *Microfluidics and Nanofluidics* **5**, 145–174 (2008).
- 458 21. Pearson, M. & Seyed-Yagoobi, J. Advances in electrohydrodynamic conduction pumping. *IEEE Transactions*
459 *on Dielectrics and Electrical Insulation* **16**, 424–434 (2009).
- 460 22. Darabi, J. & Wang, H. Development of an electrohydrodynamic injection micropump and its potential
461 application in pumping fluids in cryogenic cooling systems. *Journal of Microelectromechanical Systems* **14**,
462 747–755 (2005).
- 463 23. Chang, S. T., Paunov, V. N., Petsev, D. N. & Velev, O. D. Remotely powered self-propelling particles and
464 micropumps based on miniature diodes. *Nature Materials* **6**, 235–240 (2007).
- 465 24. Kim, J. W., Suzuki, T., Yokota, S. & Edamura, K. Tube-type micropump by using electro-conjugated fluid
466 (ECF). *Sensors and Actuators, A: Physical* **174**, 155–161 (2012).
- 467 25. Cacucciolo, V., Shigemune, H., Cianchetti, M., Laschi, C. & Maeda, S. Conduction Electrohydrodynamics with
468 Mobile Electrodes: A Novel Actuation System for Untethered Robots. *Advanced Science* 1600495 (2017).
- 469 26. Wehner, M. *et al.* Pneumatic Energy Sources for Autonomous and Wearable Soft Robotics. *Soft Robotics* **1**,
470 263–274 (2014).
- 471 27. Rosset, S. & Shea, H. R. Flexible and stretchable electrodes for dielectric elastomer actuators. *Appl. Phys. A*
472 **110**, 281–307 (2013).
- 473 28. Shintake, J., Rosset, S., Schubert, B., Floreano, D. & Shea, H. Versatile Soft Grippers with Intrinsic
474 Electroadhesion Based on Multifunctional Polymer Actuators. *Advanced Materials* **28**, 231–238 (2016).

- 475 29. Wehner, M. *et al.* An integrated design and fabrication strategy for entirely soft, autonomous robots. *Nature*
476 **536**, 451–455 (2016).
- 477 30. Laser, D. J. & Santiago, J. G. A review of micropumps. *Journal of Micromechanics and Microengineering* **14**,
478 R35–R64 (2004).
- 479 31. Wang, Y.-N. & Fu, L.-M. Micropumps and biomedical applications – A review. *Microelectronic Engineering*
480 **195**, 121–138 (2018).
- 481

482 **ADDITIONAL REFERENCES**

- 483
- 484 32. Rosset, S., Araromi, O. A., Schlatter, S. & Shea, H. R. Fabrication Process of Silicone-based Dielectric
485 Elastomer Actuators. *Journal of Visualized Experiments* 1–13 (2016).
- 486 33. Schlatter, S., Illenberger, P. & Rosset, S. Peta-pico-Voltron: An open-source high voltage power supply.
487 *HardwareX* **4**, e00039 (2018).
- 488 34. MGD 1000S. Available at: <https://www.micropumps.co.uk/TCSMGD1000range.htm>.
- 489 35. McMaster STPAC. Available at: <https://www.mcmaster.com/9965k62>.
- 490 36. Olsson, A., Enoksson, P., Stemme, G. & Stemme, E. Micromachined flat-walled valveless diffuser pumps.
491 *Journal of Microelectromechanical Systems* **6**, 161–166 (1997).
- 492 37. Jang, L.-S. *et al.* A stand-alone peristaltic micropump based on piezoelectric actuation. *Biomed Microdevices* **9**,
493 185–194 (2007).
- 494 38. Lei, K. F. *et al.* A vortex pump-based optically-transparent microfluidic platform for biotech and medical
495 applications. *Proc Inst Mech Eng H* **221**, 129–141 (2007).
- 496 39. Kawun, P., Leahy, S. & Lai, Y. A thin PDMS nozzle/diffuser micropump for biomedical applications. *Sensors*
497 *and Actuators A: Physical* **249**, 149–154 (2016).
- 498 40. Richter, A., Plettner, A., Hofmann, K. A. & Sandmaier, H. A micromachined electrohydrodynamic (EHD)
499 pump. *Sensors and Actuators A: Physical* **29**, 159–168 (1991).
- 500 41. Ahn, S.-H. & Kim, Y.-K. Fabrication and experiment of a planar micro ion drag pump. *Sensors and Actuators*
501 *A: Physical* **70**, 1–5 (1998).
- 502 42. Chen, L., Wang, H., Ma, J., Wang, C. & Guan, Y. Fabrication and characterization of a multi-stage
503 electroosmotic pump for liquid delivery. *Sensors and Actuators, B: Chemical* **104**, 117–123 (2005).
- 504 43. Chuan-Hua Chen & Santiago, J. G. A planar electroosmotic micropump. *Journal of Microelectromechanical*
505 *Systems* **11**, 672–683 (2002).
- 506 44. Zengerle, R., Ulrich, J., Kluge, S., Richter, M. & Richter, A. A bidirectional silicon micropump. *Sensors and*
507 *Actuators A: Physical* **50**, 81–86 (1995).
- 508 45. Homsy, A., Linder, V., Lucklum, F. & de Rooij, N. F. Magnetohydrodynamic pumping in nuclear magnetic
509 resonance environments. *Sensors and Actuators B: Chemical* **123**, 636–646 (2007).
- 510 46. Ashouri, M., Shafii, M. B. & Moosavi, A. Theoretical and experimental studies of a magnetically actuated
511 valveless micropump. *J. Micromech. Microeng.* **27**, 015016 (2016).

- 512 47. Tanaka, Y., Noguchi, Y., Yalikul, Y. & Kamamichi, N. Earthworm muscle driven bio-micropump. *Sensors and*
513 *Actuators B: Chemical* **242**, 1186–1192 (2017).
- 514 48. Van de Pol, F. C. M., Van Lintel, H. T. G., Elwenspoek, M. & Fluitman, J. H. J. A thermopneumatic
515 micropump based on micro-engineering techniques. *Sensors and Actuators A: Physical* **21**, 198–202 (1990).
- 516 49. Sim, W. Y., Yoon, H. J., Jeong, O. C. & Yang, S. S. A phase-change type micropump with aluminum flap
517 valves. *J. Micromech. Microeng.* **13**, 286–294 (2003).
- 518 50. Jung, J.-Y. & Kwak, H.-Y. Fabrication and testing of bubble powered micropumps using embedded
519 microheater. *Microfluid Nanofluid* **3**, 161–169 (2007).
- 520 51. Shaegh, S. A. M. *et al.* Plug-and-play microvalve and micropump for rapid integration with microfluidic chips.
521 *Microfluid Nanofluid* **19**, 557–564 (2015).
- 522 52. Jeong, O. C., Park, S. W., Yang, S. S. & Pak, J. J. Fabrication of a peristaltic PDMS micropump. *Sensors and*
523 *Actuators A: Physical* **123–124**, 453–458 (2005).
- 524 53. Jahanshahi, A., Axisa, F. & Vanfleteren, J. Fabrication of an implantable stretchable electro-osmosis pump. in
525 *Microfluidics, BioMEMS, and Medical Microsystems IX* **7929**, 79290R (International Society for Optics and
526 Photonics, 2011).
- 527 54. Stergiopoulos, C., Vogt, D., Tolley, M. & Wehner, M. a Soft Combustion-Driven Pump for Soft Robots.
528 *Proceedings of the ASME 2014 Conference on Smart Materials, Adaptive Structures and Intelligent Systems*
529 *SMASIS2014* 1–6 (2014).
- 530 55. Murray, B. C. M. *et al.* Poroelastic Foams for Simple Fabrication of Complex Soft Robots. *Advanced Materials*
531 **27**, 6334–6340 (2015).
- 532 56. Loepfe, M., Schumacher, C. M. & Stark, W. J. Design, Performance and Reinforcement of Bearing-Free Soft
533 Silicone Combustion-Driven Pumps. *Ind. Eng. Chem. Res.* **53**, 12519–12526 (2014).

534

535 **Acknowledgments:** We are grateful to H. Shigemune for discussions about EHD, to M. Imboden
536 for assistance with the thermal regulation experiments, and to O. Gudozhnik for developing the 5
537 and 6 kV supply weighing 16-20 g. We acknowledge financial support from JSPS KAKENHI
538 under Grants 16H04306, 18H05473, and 19H05328; MEXT/JSPS under Leading Initiative for
539 Excellent Young Researchers; Swiss National Science Foundation through NCCR Robotics;
540 Japanese TOBITATE! Young Ambassador Program; Hasler Foundation Cyber-Human Systems
541 program; the BioRobotics Institute of Scuola Superiore Sant'Anna, Pisa in the person of Cecilia
542 Laschi for Vito Cacucciolo's initial visit to EPFL.

543 **Author contributions:** V.C., J.S., S.M., D.F., and H.S. conceived the project. V.C. and J.S.
544 designed and characterised the devices. V.C., J.S. and Y.K. fabricated the devices. V.C. and H.S.
545 analysed the data. S.M., H.S. and D.F. contributed to data interpretation. V.C., J.S. and H.S. wrote
546 the paper. All authors provided feedback and agree with the final version of the manuscript.

547
548 The authors declare the following competing financial interest(s): V.C., J.S., S.M., D.F., and H.S.
549 declare financial interest in form of a patent application.

550